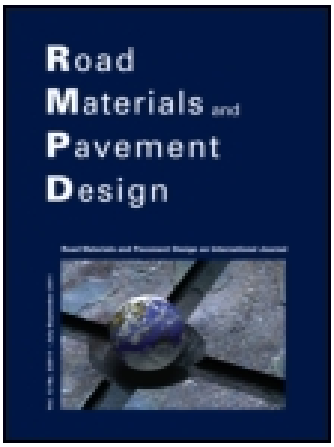

Road Materials and Pavement Design
Publication details, including instructions for authors and subscription information:
http://www.tandfonline.com/loi/trmp20

Experimental evaluation and theoretical analysis of multi-layered road cumulative deformation under dynamic loads

Zheng Lu[a], Hai-lin Yao[a], Jie Liu[a] & Zhi Hu[a]
[a] State Key Laboratory of Geomechanics and Geotechnical Engineering, Institute of Rock and Soil Mechanics, Chinese Academy of Sciences, Wuhan 430071, People's Republic of China
Published online: 28 Oct 2013.

To cite this article: Zheng Lu, Hai-lin Yao, Jie Liu & Zhi Hu (2014) Experimental evaluation and theoretical analysis of multi-layered road cumulative deformation under dynamic loads, Road Materials and Pavement Design, 15:1, 35-54, DOI: 10.1080/14680629.2013.852609

To link to this article: http://dx.doi.org/10.1080/14680629.2013.852609

Road Materials and Pavement Design, 2014
Vol. 15, No. 1, 35–54, http://dx.doi.org/10.1080/14680629.2013.852609

Taylor & Francis
Taylor & Francis Group

Experimental evaluation and theoretical analysis of multi-layered road cumulative deformation under dynamic loads

Zheng Lu*, Hai-lin Yao, Jie Liu and Zhi Hu

State Key Laboratory of Geomechanics and Geotechnical Engineering, Institute of Rock and Soil Mechanics, Chinese Academy of Sciences, Wuhan 430071, People's Republic of China

Excessive deformation of multi-layered road structure induced by vehicle traffic loading is one of the main reasons leading to pavement failure. In this paper, the elastic response and cumulative deformation of a multi-layered road structure under dynamic loads are investigated through experimental tests and theoretical analysis. First, a physical model with thin asphalt surfacing layer, cement stabilised gravel road base and layered decomposed granite soil subgrade is built to better understand the dynamic behaviour of a multi-layered road structure system. Experiments are performed to determine the elastic responses (vertical stress and displacement) and cumulative plastic deformation at different depths of road structures. A calculation method of the dynamic stiffness matrix is developed on the basis of an assembly process compatible with good numerical efficiency, and results from the calculations are verified using model experiment data. Then, the dynamic deviator stress is derived according to the dynamic stiffness matrix method and is used to formulate a cumulative deformation computational model considering both road infrastructure and its soft subsoil. Moreover, the cumulative deformation of a road on soft subsoil under repeated traffic load is analysed for different material properties of the road layers using the presented method.

Keywords: cumulative deformation; dynamic stiffness matrix; soft subsoil; experiment; pavement; dynamic loads

1. Introduction

For a road constructed on natural subsoil or soft subsoil, the cumulative plastic deformation of the pavement, subgrade and the subsoil due to vehicle traffic load is one of the important factors that control the long-term service life as well as the maintenance cost of the road. Therefore, it is essential to predict the traffic load-induced cumulative deformation so as to carry traffic safely, conveniently and economically during its entire lifespan. Generally speaking, there are three factors affecting the traffic load-induced cumulative deformation, (1) the traffic volume and magnitude of axle loads, (2) the thickness and physical and mechanical properties of pavement and subgrade, (3) the dynamic strength and deformation characteristics of the natural subsoil or soft subsoil. During the last decades, the analysis and design of road pavement and subgrade have traditionally relied on past experience and empirical methods which are developed on the basis of the static mechanical conditions, such as China Specifications for Design Highway Asphalt Pavement (2006) and China Technical Specifications for Design and Construction of Highway Embankment on Soft Ground (1996). However, the permanent deformation of road structure is obviously due to the application of moving repeated traffic loading. More recently, researchers have introduced a variety of different methods to predict the cumulative deformation of pavement,

*Corresponding author. Email: lzwhrsm@163.com

subgrade and the subsoil of a road (Francois, Karg, Degrande, & Haegeman, 2010; Hu, 2010; Joseph & James, 2012; Kettil, Lenhof, & Runesson, 2007). However, any reasonable cumulative deformation prediction method should consider the above-mentioned factors directly or indirectly.

Early work on the analysis and prediction of road cumulative deformation caused by repeated loading were based on experiments, which make it possible to derive empirical relationships giving, for instance, the amount of cumulative deformation as a function of the number of applied load cycles. A number of empirical equations have been proposed to predict the permanent deformation of soft soil under repeated load. Among them, the power equation proposed by Monismith, Ogawa, and Freeme (1975) has been widely used. Li and Selig (1996) established a similar exponential equation, in which the constants are determined by the physical state and strength of subsoil. Li and Selig (1998) provided the values of the constants of several cohesive soils by employing cyclic loading experiment, and showed some successful applications of the equation to predict the long-term settlement of cohesive soils under train loading. Chai and Miura (2002) proposed an empirical equation to calculate the permanent settlement of road on soft subsoil with a low embankment. The method suggested by Chai and Miura considers the effects of initial static deviator stress, the magnitude of traffic-load applications and the strength and compression characteristics of subsoil. However, the traffic load used by Chai and Miura is simplified as a static load. Also, the effect of cumulative deformation of road pavement and subgrade on the total settlement is not considered.

Equivalent static loading methods seem to be useful to calculate the settlement of the subsoil of road, because the classical elastic solution and consolidation theory can be easily used. For example, Kutara, Miki, and Mashita (1980) proposed a design method, in which an equivalent static load represents the traffic load, and a one-dimensional consolidation theory was used to predict the settlement. Fujikawa (1996) and Fujikawa, Miura, and Beppu (1996) assumed a triangular distribution pattern of traffic-load-induced stress increments based on field measurement. Although this method is simple, the dynamic characteristics of soils are not taken into consideration, and the traffic-load-induced stress is not calculated explicitly.

The development of computational methods has opened the possibility to perform numerical simulations of the response of road structures under repeated load. By means of dynamic numerical analysis, Hyodo, Yasuhara, and Murata (1996) investigated the deformation of the soft clay foundation of low embankment road under traffic loading. Kettil et al. (2007) presented modelling and simulation of inelastic deformation in road structures leading to rutting. In his paper, the modelling and calculating were performed through the Finite Element (FE) programme Abaqus. Mulungye, Owende, and Mellon (2007) and Akbulut and Aslantas (2005) evaluated the effect of tyre pressure, wheel configuration and axle load variations of a truck on the structural performance of a flexible road pavement with thin surfacing layer, base course and subgrade using the finite element method. Manzari and Prachathananukit (2001), Lu and Wright (1998) and Zeng, Olsson, and Wiberg (2000) also calculated the cumulative plastic deformation of road structures subjected to cyclic mechanical loads by introducing different elastoplastic material models. Theoretically, explicit simulation is preferable. However, it would consist of implementing a conventional step-by-step elastoplastic procedure, requiring the discretisation of each individual load cycle into a sufficiently small number of cycles, which will quite rapidly lead to considerable computational time and complete loss of numerical accuracy as the number of cycles increases.

A review of the literature shows that a cumulative deformation analysis of a layered road structure can be conducted using empirical, empirical/numerical or purely numerical methods, and most of the available works on the subject, though there are not many, are rather theoretical and lack calibration on the basis of experimental measures. Thus, the results of these approaches are rather qualitative, and even though they help to understand the system behaviour, they cannot be used directly in the design. In fact, experimental measurements can increase understanding of

the phenomena intuitively and provide predictions that can be utilised to improve the design and maintenance and, hence, reduce costs.

The objective of this work is therefore to investigate the cumulative plastic deformation of a multi-layered road structure under dynamic repeated loads based on physical model experimental measurements and theoretical analysis, with consideration of the cumulative plastic deformation of both road infrastructure and its subsoil. The traffic-load-induced stress, which is very important in predicting cumulative deformation of the subsoil, is calculated explicitly by developing a dynamic stiffness matrix method and verified through experimental measurements. A computational model is proposed to calculate the cumulative plastic deformation of all the road structure layers and the subsoil. The new model included two parts: one is the deformation of the road structure layers themselves Sp_1, which is calculated according to the physical model experiment directly. The other is the deformation of the underlying soft ground Sp_2, and it is determined by the theoretical equation of cumulative deformation in which the dynamic deviator stress, the number of repeated loadings and the material properties of soft subsoil are considered. Furthermore, a parametric study is conducted to consider the influence of the different material properties of the multi-layered road structure on the total cumulative plastic deformation using numerical computation.

2. Experimental investigation

2.1. *Materials of multi-layered road structure*

Figure 1 shows the laboratory physical model experiment that represents the typical multi-layered road structures that are built to simulate the dynamic response of a road subjected to vehicle traffic loads. The model includes, from bottom to top, a layer of subgrade (completely decomposed granite whose properties are shown in Table 1) at a height of 1.05 m compacted into three layers with heights of 0.45, 0.3 and 0.3 m, respectively, a layer of sub-base at a height of 0.3 m composed of cement-stabilised gravel at a 4% cement content, a layer of base at a height of 0.3 m composed of cement-stabilised gravel with 6% cement content and an asphalt surface layer at a height of 0.18 m to simulate a flexible pavement on which the loading equipment is placed with respect to the position of the loading plate. The structure layers are constrained at two opposite sides by inclined planes (slopes) that represent free edges. The other sides are constrained by vertical steel baffle plates representing the beginning and the end of the model. The loading equipment is fixed on a reaction beam, which is bolted onto the steel frame. All components of the experiment are located on a reinforced concrete foundation that is able to support the important weights of these components.

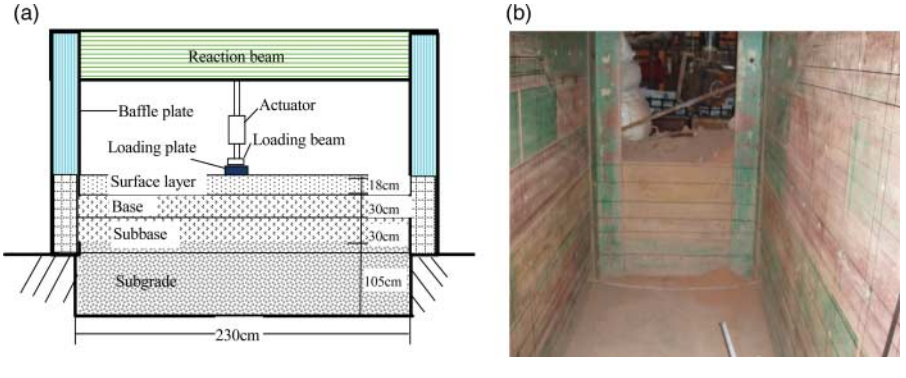

Figure 1. (a) Representation of physical model, (b) physical model box.

Table 1. Material properties of filled subgrade.

Soil type	CBR (%)	Specific gravity	Liquid limit (%)	Plastic limit (%)	Plasticity index	Optimum moisture content (%)	Maximum dry density (kg/m^3)
Low liquid-limit clay	8.9	2.70	34.1	24.6	9.5	10.2	1944

Table 2. Physical and mechanical characteristics of the road structure layers.

Layers	Elastic modulus (MPa)	Poisson ratio	Thickness (m)	Density (kg/m^3)
Surface layer	1400.00	0.30	0.18	2400
Base	734.63	0.30	0.30	2230
Subbase	636.58	0.30	0.30	2195
Subgrade layer 1	45.15	0.35	0.30	1981
Subgrade layer 2	28.88	0.35	0.30	1992
Subgrade layer 3	36.45	0.35	0.45	1955

The physical and mechanical characteristics of the road structure layers are obtained according to the laboratory tests and are shown in Tables 1 and 2. The indoors tests include compaction, liquid and plastic limit, specific gravity, California bearing ratio (CBR) and modulus test, which are all conducted on the basis of the China Test method of soils for Highway Engineering (JTG E40-2007). In order to minimise the influence of temperature on the tests, all the experiments including modulus measure were done in a closed laboratory whose temperature was fixed at 25°C.

2.2. *Testing methods*

In this experiment, the effect of double-wheel loading is taken into consideration to simulate the vehicle loads, as shown in Figure 2, and the distribution of the loads meets the requirements set by the Specifications for Design Highway Asphalt Pavement of China (2006). The loading equipment consisted of, from bottom to top, rubber bearings, steel plates, a loading beam and an actuator. The shape of the tyre-pavement contact area is assumed to be circular, and the load pressure within the contact area is assumed to be uniformly distributed. According to Design Highway Asphalt Pavement of China (2006), the diameter of circular contact d is 0.213 m, and the force and pressure induced by a single load are 25 kN and 0.7 MPa, respectively, corresponding to the static conditions. The distance between the two circles is 1.5d.

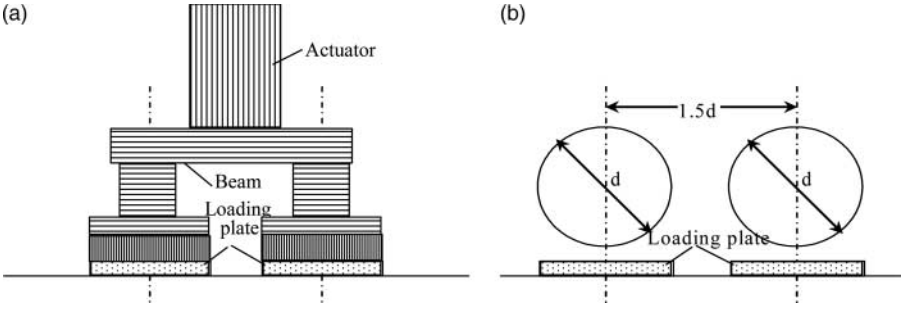

Figure 2. (a) Loading equipment, (b) distribution of the loads.

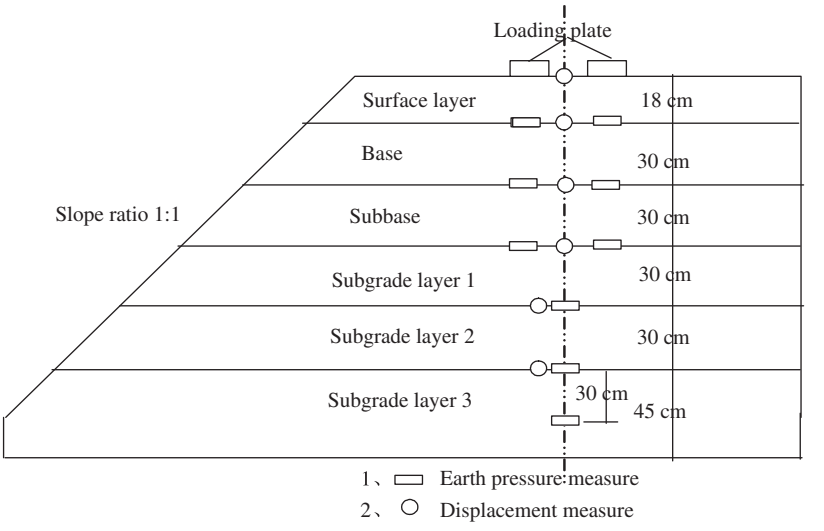

Figure 3. Measuring points of earth pressure and displacement.

The detailed size of the model is as follows: the longitudinal length is 2.3 m, the horizontal width of the top is 2.0 m, the horizontal width of the bottom is 3.6 m and the slope ratio is 1:1, as shown in Figure 3. Different transducers are installed in the model of the road structures to measure the stresses and displacements. According to the test aims and requirements, the measuring sensors are used as follows: (1) Earth pressure cell with resistance straingauge: measuring range 0–2 MPa with a sensitivity of 1 kPa. (2) Linear Variable Differential Transformer (LVDT) displacement transducer: measuring range ±12.5 mm with a precision ratio of 0.1%. All the transducers are installed at the bottom of each structure layer, as shown in Figure 3. These transducers and their cables are protected by aluminium tubes to prevent damage from cyclic loadings.

A typical experiment generated signals of a semi-sinusoidal wave that simulates the passage of traffic vehicles. If a truck is moving on a rough pavement surface, there will be a variation in the load amplitude imposed by the truck. According to Yao, Lu, and Luo (2009), the impact coefficient (the ratio of the amplitude of the dynamic load to the static load) of the highway pavement, whose roughness index is no more than IRI 2 mm, is between 1.2 and 1.5. Therefore, the maximum dynamic load amplitude of the double wheels is determined to be 1.5 times the static load. To simulate multi-stage loading, the experiment contains several stages, where every stage consists of 1000 cycles and corresponded to a frequency, as shown in Table 3. This experiment is denoted as "DT", whose purpose is to study the effect of the traffic load amplitudes and frequencies on the dynamic characteristics of the road structure layers.

To obtain the cumulative deformation of the road structure layers under long-term, repeated vehicle loads, an additional experiment, denoted by "CT", is performed where the dynamic load amplitude is 75 kN and the frequency is 7 Hz and consists of 10^6 cycles.

Table 3. Load amplitude and frequency of multi-stage loading.

Load amplitude (kN)	15	20	25	30	45	50	55	60	65	70	75	75	75	75	75	75
Load frequency (Hz)	2	2	2	2	2	2	2	2	2	2	2	3	4	5	6	7

2.3. *Experimental results*

The "DT" experiment is conducted with respect to the effects of depth, load amplitude and load frequency on the vertical stress and elastic displacement of the road structure layers. Several test results are presented in Table 4. It can be seen from Table 4 that the vertical stress and displacement at the top of each layer decrease with depth. The values of elastic response decrease sharply in the initial range at a depth of 0.78 m, then gradually decrease to zero when the depth is greater than 0.78 m. The ratios of the stresses at the base top, sub-base top and subgrade top to the top of surface layer are 83.67%, 28.05% and 4.23%, respectively, which indicates that the majority of the stresses caused by vehicle loads are imposed and dispersed by the road pavement.

The effects of the load magnitude and the number of loading cycles on the cumulative deformation (irreversible permanent deformation) of the road structure layers are also investigated in the "CT" experiment, and the results are shown in Figures 4 and 5. The cumulative deformation of each layer is the difference between the cumulative deformation of the top and bottom of the layer. It can be seen from Figure 4 that the relationships between the cumulative deformation and the load magnitude of all the layers are approximately linear. It is worth noting that the increase in the law of cumulative deformation as the number of applied load cycles increases is extremely important in the study of the dynamic behaviour of road structures. Therefore, the effect of the number of loading cycles on the cumulative deformation is investigated, as shown in Figure 5. As can be seen, the cumulative deformation of each layer exhibits the same tendency; the cumulative deformation increases with the number of cycles until one million cycles is reached. The cumulative deformation occurs rapidly for a short number of cycles and becomes much lower at other moments. These rapid deformations are a result of the reorganisation of grains of the road structure layers. It can also be observed from Figure 5 that the cumulative deformation of each layer of the road under repeated loadings can be estimated by exponential formula, $S_p = \kappa N^{\chi} h$, where

Table 4. Elastic response measurements of the road structures (load amplitude is 75 kN and frequency is 7 Hz).

	Depth (m)						
Elastic response	0.0	0.18	0.48	0.78	1.08	1.38	1.68
Vertical stress (MPa)	1.041	0.871	0.292	0.044	0.023	0.009	0.004
Vertical displacement (mm)	0.403	0.312	0.219	0.153	0.088	0.055	N/A

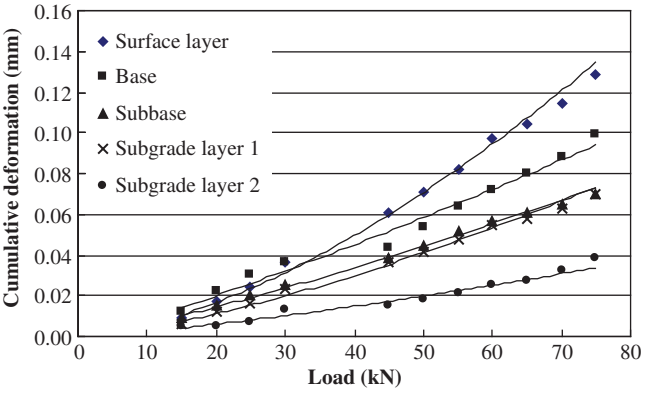

Figure 4. Variation of cumulative deformation with load amplitude (load frequency is 2 Hz).

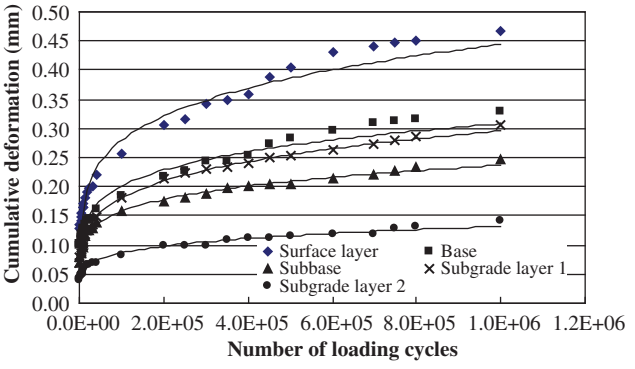

Figure 5. Variation of cumulative deformation with the number of cycles (load amplitude is 75 kN and frequency is 7 Hz).

Table 5. Experimental parameters κ and χ for each layer.

Experimental parameters	Surface layer	Base	Subbase	Subgrade 1	Subgrade 2
$\kappa(\times 10^{-2})$	2.77	2.42	2.10	1.52	1.05
$\chi(\times 10^{-1})$	2.00	1.84	1.75	2.15	1.82

S_p denotes the cumulative deformation, h is the thickness of road structure layer, N represents the number of loading cycles, and κ and χ are two experimental parameters shown in Table 5 for this situation. It is obvious that the relationship between the cumulative deformation and the number of cycles can be exactly described by the exponential formula in terms of the presented road materials.

3. Theoretical investigation

3.1. *Dynamic elastic response of multi-layered road structure*

A road structure is a multi-layered system composed of pavement, base, sub-base and combined unbound aggregate subgrade, on a foundation of natural soil or bedrock. Therefore, a multi-layered elastodynamic model could be used to analyse the stresses and displacements of a road structure due to vehicle loads. A calculation method of the dynamic stiffness matrix is developed on the basis of the stress and displacement matrices and the boundary conditions as well as the continuity conditions at the interface. The general solutions are derived and the dynamic calculations are used to predict the elastic response of the portion under the passages of vehicles. All the experiment layers are considered as following the linear elastic constitutive law. Although the configuration of the loading experiment is non-axisymmetric, the single-circle load case can be considered as an axisymmetric problem and be used to analyse the response first. Then, the double-circle load case can be made by invoking the principle of superposition, to simulate the experimental loading. For the case of single-circle load, it is convenient to use a polar co-ordinate system (r, θ, z), which is represented in Figure 6.

For symmetric wave motion about the z-axis, the displacements are independent of the θ coordinate. Excluding the rotational motion, the displacement field, $u = [u_r, 0, u_z]$, and the stress components, $(\sigma_{rr}, \sigma_{\theta\theta}, \sigma_{zz}, \sigma_{rz})$, of a homogeneous isotropic elastic solid are determined from two

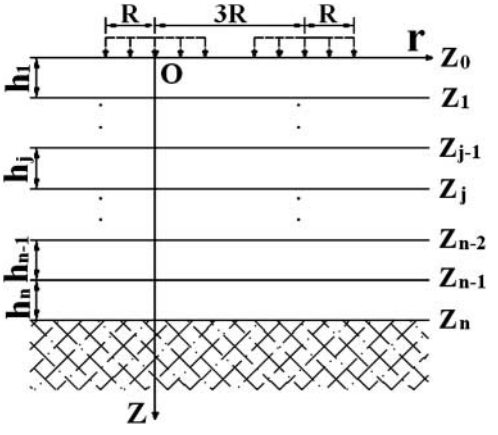

Figure 6. Geometry and coordinates in a multi-layered road structure.

potentials $\phi(r,z,t)$ and $\psi(r,z,t)$ as follows (Su, Tian, & Pao, 2002):

$$u_r = \frac{\partial \phi}{\partial r} + \frac{\partial^2 \psi}{\partial r \partial z}, \tag{1}$$

$$u_z = \frac{\partial \phi}{\partial z} - \frac{\partial^2 \psi}{\partial r^2} - \frac{1}{r}\frac{\partial \psi}{\partial r}, \tag{2}$$

$$\sigma_{zz} = \lambda \nabla^2 \phi + 2\mu \left(\frac{\partial^2 \phi}{\partial z^2} - \frac{\partial^3 \psi}{\partial z \partial r^2} - \frac{1}{r}\frac{\partial^2 \psi}{\partial z \partial r} \right), \tag{3}$$

$$\sigma_{rz} = \mu \left(2\frac{\partial^2 \phi}{\partial r \partial z} + 2\frac{\partial^3 \psi}{\partial r \partial z^2} - \frac{\partial}{\partial r}\nabla^2 \psi \right), \tag{4}$$

$$\sigma_{rr} = \lambda \nabla^2 \phi + 2\mu \left(\frac{\partial^2 \phi}{\partial r^2} + \frac{\partial^3 \psi}{\partial r^2 \partial z} \right), \tag{5}$$

$$\sigma_{\theta\theta} = \lambda \nabla^2 \phi + \frac{2\mu}{r} \left(\frac{\partial \phi}{\partial r} + \frac{\partial^2 \psi}{\partial z \partial r} \right) \tag{6}$$

where the z-axis is the axis of symmetry of the solid; u_r and u_z are displacement components in the r and z directions, respectively; λ and μ are the Lame constants and $\nabla^2 = \partial^2/\partial r^2 + r^{-1}\partial/\partial r + \partial^2/\partial z^2$; ϕ is from the compression waves (particle movement in the direction of wave propagation), and ψ is from the shear waves (particle movement perpendicular to the direction of propagation) as in the following Helmholtz equations:

$$\nabla^2 \phi - \frac{1}{c_p^2}\frac{\partial^2 \phi}{\partial t^2} = 0, \tag{7}$$

$$\nabla^2 \psi - \frac{1}{c_s^2}\frac{\partial^2 \psi}{\partial t^2} = 0, \tag{8}$$

where $c_p = \sqrt{(\lambda + 2\mu)/\rho}$ and $c_s = \sqrt{\mu/\rho}$ are the compression and shear wave speed, respectively; ρ is the mass density of the solid.

According to the model experiment conducted by Section 2, the steady-state response may be introduced in this paper, and changes of the functions and variables can be performed:

$$\Omega(r,z,t) = \Omega(r,z)\,\mathrm{e}^{i\omega t}, \tag{9}$$

where $\Omega(r,z,t)$ indicates all the variables and the two potentials; e is the exponential function, and ω is the excitation frequency.

At this point, the mth order Hankel transform is introduced. Its direct and inverse forms are defined as follows (Alejandro & Rafael, 2007):

$$\bar{f}^m(\xi,z) = \int_0^\infty f(r,z) r J_m(r\xi)\,\mathrm{d}r, \tag{10}$$

$$f(r,z) = \int_0^\infty \bar{f}^m(\xi,z)\xi J_m(r\xi)\,\mathrm{d}\xi, \tag{11}$$

where $J_m(z)$ is the mth order first kind Bessel function; ξ denotes the horizontal wave-number; f is a variable in the space domain, and $\bar{f}$ is the corresponding variable in the transformed domain.

Substituting Equation (9) in Equations (7) and (8) and applying a zero-order Hankel transformation to the radial coordinate, r, the set of wave equations is reduced to a set of ordinary differential equations:

$$\frac{\mathrm{d}^2\bar{\phi}^{[0]}}{\mathrm{d}z^2} - \left(\xi^2 - \frac{\omega^2}{c_\mathrm{p}^2}\right)\bar{\phi}^{[0]} = 0, \tag{12}$$

$$\frac{\mathrm{d}^2\bar{\psi}^{[0]}}{\mathrm{d}z^2} - \left(\xi^2 - \frac{\omega^2}{c_\mathrm{s}^2}\right)\bar{\psi}^{[0]} = 0, \tag{13}$$

where the superscript number in the square brace denotes the order of the Hankel transformation, and the general solution of Equations (12) and (13) may be written as

$$\bar{\phi}^{[0]} = A(\xi,z)\,\mathrm{e}^{\alpha_p(z-h)} + B(\xi,z)\,\mathrm{e}^{-\alpha_p z}, \tag{14}$$

$$\bar{\psi}^{[0]} = C(\xi,z)\,\mathrm{e}^{\alpha_s(z-h)} + D(\xi,z)\,\mathrm{e}^{-\alpha_s z}, \tag{15}$$

where $\alpha_\mathrm{p} = \sqrt{\xi^2 - k_\mathrm{p}^2}$ and $\alpha_\mathrm{s} = \sqrt{\xi^2 - k_\mathrm{s}^2}$ are the frequency-dependent complex wave number for the P-wave and S-wave with $k_\mathrm{p} = \omega/c_\mathrm{p}$ and $k_\mathrm{s} = \omega/c_\mathrm{s}$. The roots α_p and α_s are located in the first quadrant, and thus their real parts are positive. $A(\xi,z)$, $B(\xi,z)$, $C(\xi,z)$ and $D(\xi,z)$ are arbitrary functions to be determined by the boundary conditions. Because of numerical difficulties due to exponential terms in the rigidity matrix, layers must be divided into several sub-layers increasing the number of iterations. In fact, the role of the fitted phase translation is to solve this problem by excluding exponential terms (growing exponential) in the stiffness matrix thus providing good conditioning (Lefeuve-Mesgouez & Mesgouez, 2012).

By applying the zero-order or first-order Hankel transformation to Equations (1)–(6), after some mathematical manipulation with respect to the relationship between the zero-order and first-order Hankel equations, the partial differential Equations (1)–(6) are transformed into ordinary

differential equations with the vertical coordinate z as variable.

$$\bar{u}_r^{[1]} = -\xi\bar{\phi}^{[0]} - \xi\frac{\mathrm{d}\bar{\psi}^{[0]}}{z}, \tag{16}$$

$$\bar{u}_z^{[0]} = \frac{\mathrm{d}\bar{\phi}^{[0]}}{\mathrm{d}z} + \xi^2\bar{\psi}^{[0]}, \tag{17}$$

$$\bar{\sigma}_{zz}^{[0]} = \lambda\left(\frac{\mathrm{d}^2\bar{\phi}^{[0]}}{\mathrm{d}z^2} - \xi^2\bar{\phi}^{[0]}\right) + 2\mu\frac{\mathrm{d}\bar{u}_z^{[0]}}{\mathrm{d}z}, \tag{18}$$

$$\bar{\sigma}_{rz}^{[1]} = \mu\frac{\mathrm{d}\bar{u}_r^{[1]}}{\mathrm{d}z} - \mu\xi\bar{u}_z^{[0]}, \tag{19}$$

$$\bar{\Psi}_{rr}^{[0]} = \lambda\left(\frac{\mathrm{d}^2\bar{\phi}^{[0]}}{\mathrm{d}z^2} - \xi^2\bar{\phi}^{[0]}\right) + 2\mu\xi\bar{u}_r^{[1]}, \tag{20}$$

$$\bar{\Psi}_{\theta\theta}^{[0]} = \lambda\left(\frac{\mathrm{d}^2\bar{\phi}^{[0]}}{\mathrm{d}z^2} - \xi^2\bar{\phi}^{[0]}\right), \tag{21}$$

where $\Psi_{rr} = \sigma_{rr} + 2\mu u_r/r$, $\Psi_{\theta\theta} = \sigma_{\theta\theta} - 2\mu u_r/r$.

Substituting Equations (14) and (15) into Equations (16)–(19), the displacement and stress components can be derived in a matrix form as

$$\begin{Bmatrix} \bar{u}_r^{[1]} \\ \bar{u}_z^{[0]} \\ \bar{\sigma}_{zz}^{[0]} \\ \bar{\sigma}_{rz}^{[1]} \end{Bmatrix} = \begin{bmatrix} -\xi\,\mathrm{e}^{\alpha_\mathrm{p}(z-h)} & -\xi\,\mathrm{e}^{-\alpha_\mathrm{p}z} & -\xi\alpha_\mathrm{s}\,\mathrm{e}^{\alpha_\mathrm{s}(z-h)} & \xi\alpha_\mathrm{s}\,\mathrm{e}^{-\alpha_\mathrm{s}z} \\ \alpha_\mathrm{p}\,\mathrm{e}^{\alpha_\mathrm{p}(z-h)} & -\alpha_\mathrm{p}\,\mathrm{e}^{-\alpha_\mathrm{p}z} & \xi^2\,\mathrm{e}^{\alpha_\mathrm{s}(z-h)} & \xi^2\,\mathrm{e}^{-\alpha_\mathrm{s}z} \\ (2\mu\alpha_\mathrm{p}^2 - \lambda k_\mathrm{p}^2)\,\mathrm{e}^{\alpha_\mathrm{p}(z-h)} & (2\mu\alpha_\mathrm{p}^2 - \lambda k_\mathrm{p}^2)\,\mathrm{e}^{-\alpha_\mathrm{p}z} & 2\mu\xi^2\alpha_\mathrm{s}\,\mathrm{e}^{\alpha_\mathrm{s}(z-h)} & -2\mu\xi^2\alpha_\mathrm{s}\,\mathrm{e}^{-\alpha_\mathrm{s}z} \\ -2\mu\xi\alpha_\mathrm{p}\,\mathrm{e}^{\alpha_\mathrm{p}(z-h)} & 2\mu\xi\alpha_\mathrm{p}\,\mathrm{e}^{-\alpha_\mathrm{p}z} & -\mu\xi(\xi^2+\alpha_\mathrm{s}^2)\,\mathrm{e}^{\alpha_\mathrm{s}(z-h)} & -\mu\xi(\xi^2+\alpha_\mathrm{s}^2)\,\mathrm{e}^{-\alpha_\mathrm{s}z} \end{bmatrix} \cdot \begin{Bmatrix} A(\xi,z) \\ B(\xi,z) \\ C(\xi,z) \\ D(\xi,z) \end{Bmatrix}. \tag{22}$$

For a layer of thickness h, the displacements of the upper and lower boundaries can be written in terms of the constants A, B, C and D:

$$\{\bar{U}\} = \left\{\bar{u}_{r,0}^{[1]} \quad \bar{u}_{z,0}^{[0]} \quad \bar{u}_{r,h}^{[1]} \quad \bar{u}_{z,h}^{[0]}\right\} = [D]\left\{A \quad B \quad C \quad D\right\}^\mathrm{T}. \tag{23}$$

Similarly, for the same layer, stress can be expressed in terms of the previous constants:

$$\left\{\bar{\Theta}\right\} = \left\{-\bar{\sigma}_{zz,0}^{[0]} \quad -\bar{\sigma}_{rz,0}^{[1]} \quad \bar{\sigma}_{zz,h}^{[0]} \quad \bar{\sigma}_{rz,h}^{[1]}\right\} = [S]\left\{A \quad B \quad C \quad D\right\}^\mathrm{T}. \tag{24}$$

Using Equations (23) and (24), the following relations are obtained:

$$\{\bar{\Theta}\} = [S][D]^{-1}\{\bar{U}\} = [R]\{\bar{U}\}, \tag{25}$$

where the matrices $[D]$, $[S]$ and $[R]$, whose size is 4×4 are the displacement matrix, stress matrix and stiffness matrix of the elastic layer, respectively, and they are detailed as follows:

$$[D] = \begin{bmatrix} -\xi\, \mathrm{e}^{-\alpha_\mathrm{p} h} & -\xi & -\xi\alpha_\mathrm{s}\, \mathrm{e}^{-\alpha_\mathrm{s} h} & \xi\alpha_\mathrm{s} \\ \alpha_\mathrm{p}\, \mathrm{e}^{-\alpha_\mathrm{p} h} & -\alpha_\mathrm{p} & \xi^2\, \mathrm{e}^{-\alpha_\mathrm{s} h} & \xi^2 \\ -\xi & -\xi\, \mathrm{e}^{-\alpha_\mathrm{p} h} & -\xi\alpha_\mathrm{s} & \xi\alpha_\mathrm{s}\, \mathrm{e}^{-\alpha_\mathrm{s} h} \\ \alpha_\mathrm{p} & -\alpha_\mathrm{p}\, \mathrm{e}^{-\alpha_\mathrm{p} h} & \xi^2 & \xi^2\, \mathrm{e}^{-\alpha_\mathrm{s} h} \end{bmatrix}, \tag{26}$$

$$[S] = \begin{bmatrix} -(2\mu\alpha_\mathrm{p}^2 - \lambda k_\mathrm{p}^2)\, \mathrm{e}^{-\alpha_\mathrm{p} h} & -(2\mu\alpha_\mathrm{p}^2 - \lambda k_\mathrm{p}^2) & -2\mu\xi^2\alpha_\mathrm{s}\, \mathrm{e}^{-\alpha_\mathrm{s} h} & 2\mu\xi^2\alpha_\mathrm{s} \\ 2\mu\xi\alpha_\mathrm{p}\, \mathrm{e}^{-\alpha_\mathrm{p} h} & -2\mu\xi\alpha_\mathrm{p} & \mu\xi(\xi^2 + \alpha_\mathrm{s}^2)\, \mathrm{e}^{-\alpha_\mathrm{s} h} & \mu\xi(\xi^2 + \alpha_\mathrm{s}^2) \\ (2\mu\alpha_\mathrm{p}^2 - \lambda k_\mathrm{p}^2) & (2\mu\alpha_\mathrm{p}^2 - \lambda k_\mathrm{p}^2)\, \mathrm{e}^{-\alpha_\mathrm{p} h} & 2\mu\xi^2\alpha_\mathrm{s} & -2\mu\xi^2\alpha_\mathrm{s}\, \mathrm{e}^{-\alpha_\mathrm{s} h} \\ -2\mu\xi\alpha_\mathrm{p} & 2\mu\xi\alpha_\mathrm{p}\, \mathrm{e}^{-\alpha_\mathrm{p} h} & -\mu\xi(\xi^2 + \alpha_\mathrm{s}^2) & -\mu\xi(\xi^2 + \alpha_\mathrm{s}^2)\, \mathrm{e}^{-\alpha_\mathrm{s} h} \end{bmatrix}. \tag{27}$$

A standard assembling technique between the layers, with the continuity of the displacements and the stresses between each layer, is applied. If the road structure is built on rigid bedrock, namely the thickness of last layer is infinite, the displacements at the bottom of the Nth layer can be considered as zero. If the last layer of road structures is half space, there are no propagating waves in negative z direction (no reflection), the system is reduced to the following expression:

$$[R_\mathrm{hs}]\{\bar{U}\}_{z=z_n} = \{\bar{\Theta}\}_{z=z_n}, \tag{28}$$

where $[R_\mathrm{hs}] = [S_\mathrm{hs}][D_\mathrm{hs}]^{-1}$ and hs stands for "half space". $[D_\mathrm{hs}]$ and $[S_\mathrm{hs}]$ are the displacement matrix and stress matrix of the half space, respectively, and they are detailed as follows:

$$[D_\mathrm{hs}] = \begin{bmatrix} -\xi & \xi\alpha_\mathrm{s} \\ -\alpha_\mathrm{p} & \xi^2 \end{bmatrix}, \tag{29}$$

$$[S_\mathrm{hs}] = \begin{bmatrix} -(2\mu\alpha_\mathrm{p}^2 - \lambda k_\mathrm{p}^2) & 2\mu\xi^2\alpha_\mathrm{s} \\ -2\mu\xi\alpha_\mathrm{p} & \mu\xi(\xi^2 + \alpha_\mathrm{s}^2) \end{bmatrix}. \tag{30}$$

$[R_\mathrm{hs}]$ is assembled to the global matrix in the 2×2 right bottom sub-matrix. The assembling technique yields the following global system:

$$[R_\mathrm{global}]_{2(n+1)\times 2(n+1)} \begin{Bmatrix} \bar{U}_{z=z_0} \\ \bar{U}_{z=z_1} \\ \vdots \\ \bar{U}_{z=z_{n-1}} \\ \bar{U}_{z=z_n} \end{Bmatrix} = \begin{Bmatrix} \bar{\Theta}_{z=z_0} \\ \bar{\Theta}_{z=z_1} \\ \vdots \\ \bar{\Theta}_{z=z_{n-1}} \\ \bar{\Theta}_{z=z_n} \end{Bmatrix}. \tag{31}$$

In terms of the model experiment in this paper, the vertical loads $F(r, t)$ are distributed over a circle with radius R (Figure 2), and if the excitation frequency is ω, then the loads can be represented

as follows:

$$F(r,t) = \begin{cases} \dfrac{P\, e^{\mathrm{i}\omega t}}{\pi R^2} & |r| \le R \\ 0 & |r| > R, \end{cases} \tag{32}$$

where P is the pressure of the circular load.

By applying the zero-order Hankel transformation to Equation (32), the following equation is obtained:

$$\bar{F}^{[0]}(\xi,t) = \bar{F}^{[0]}(\xi)\, e^{\mathrm{i}\omega t} = \frac{PJ_1(R\xi)}{\pi R\xi}\, e^{\mathrm{i}\omega t}. \tag{33}$$

By invoking the principle of superposition, the double-circle load case can be made to simulate the experimental loading. In terms of the surface boundary conditions, the following relation, omitting the common time factor $\mathrm{e}^{\mathrm{i}\omega t}$, is obtained from Equations (31) and (33)

$$\begin{Bmatrix} \bar{u}^{[1]}_{r,0} \\ \bar{u}^{[0]}_{z,0} \\ \vdots \\ \bar{u}^{[1]}_{r,z_n} \\ \bar{u}^{[0]}_{z,z_n} \end{Bmatrix} = [R_{\text{global}}]^{-1} \begin{Bmatrix} -\bar{\sigma}^{[0]}_{zz,0} \\ -\bar{\sigma}^{[1]}_{rz,0} \\ \vdots \\ \bar{\sigma}^{[0]}_{zz,z_n} \\ \bar{\sigma}^{[1]}_{rz,z_n} \end{Bmatrix} = [B_{\text{global}}] \begin{Bmatrix} -\bar{F}^{[0]}(\xi) \\ 0 \\ \vdots \\ 0 \\ 0 \end{Bmatrix}, \tag{34}$$

where $[B_{\text{global}}]$ is the inverse stiffness matrix for a multi-layered road structure.

One can obtain the displacements in the wavenumber domain over the road surface and in depth according to Equation (34). Then it is rather straightforward to obtain all the transformed stress vectors in an arbitrary layer. Once the transformed stress and displacement components are determined, the actual medium response can be established by means of the Hankel inversion theorem from Equation (11). It should be noted that all the exponential functions involved in the present formulation contain only non-positive exponents, which are critical for numerical stability.

Clearly, numerical analysis is necessary to compute the stresses and displacements analytically using Equation (11). In this work, the inverse Hankel's transform in Equation (11) is evaluated by a numerical method used in Ferrari, Perciante, and Dubra (1999) and Wang and Ishikawa (2002).

3.2. *Verification of the elastic response*

The components of dynamic response solved above are very important in predicting the cumulative deformation of road structures. Thus it is necessary to verify the theoretical solutions with experimental measurements. A computing model of a multi-layered road structure is built by assuming that all the road structure layers are continuous and a linear elastic medium. Then, the dynamic stiffness matrix solutions derived in Section 3.1 are employed for the calculations. The physical and mechanical characteristics of road structure layers are obtained according to laboratory tests, and are shown in Table 2. The loading conditions and the calculative parameters are consistent with that of the "DT" experiment. The calculation points are the same as the measuring points shown in Figure 3. Figures 7–9 compare the vertical stress and displacement obtained from experiment measurements with that calculated by theoretical solutions.

From Figures 7 and 8, it can be seen that the calculated vertical stress and displacement are slightly less than those of the experimental ones in the superficial layer of road structures. This

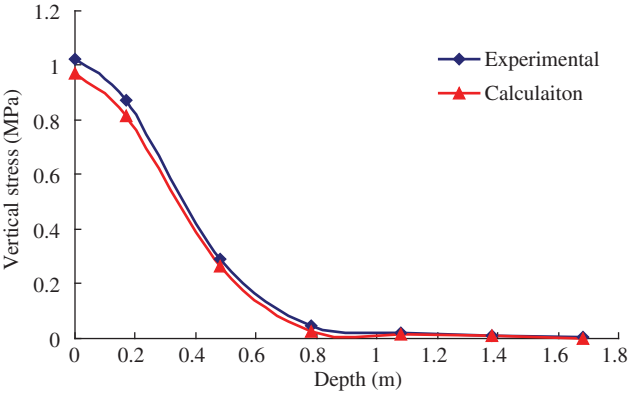

Figure 7. Comparison of the calculated vertical stress with the experimental results (load amplitude is 75 kN and frequency is 7 Hz).

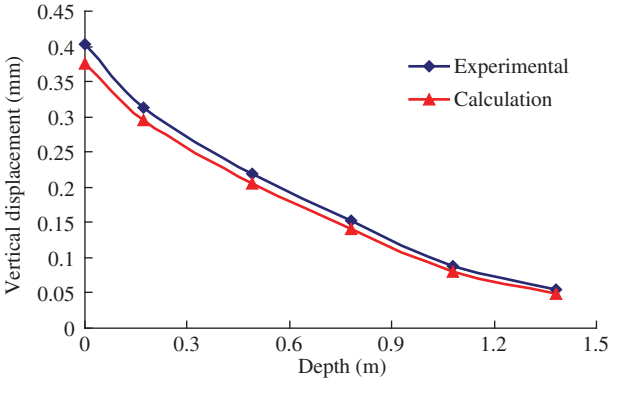

Figure 8. Comparison of the calculated vertical displacement with the experimental results (load amplitude is 75 kN and frequency is 7 Hz).

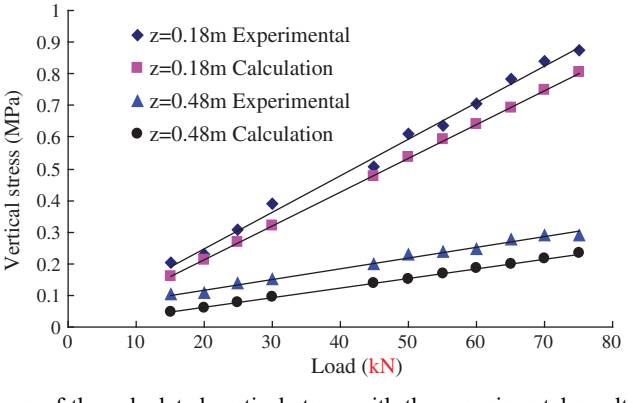

Figure 9. Comparison of the calculated vertical stress with the experimental results (load amplitude is 2 Hz).

difference between the numerical and experimental results is related to several factors, including nonlinear soil behaviour, viscoelasticity of the asphalt concrete, wave reflection on the physical model edge and the reliance on inappropriate parameters of various materials. However, the total trends generated by the theoretical calculation are in good agreement with those of the experimental trends.

A comparison of the variation of vertical stress with increasing load amplitude of calculation and that of experimental results is presented in Figure 9, where $z = 0.18$ m and $z = 0.48$ m are considered. As can be seen, the agreement between the two results, as far as the vertical stress is concerned, is excellent. The agreement between the numerical and the experimental results is good, which indicates that the dynamic stiffness matrix method is useful in predicting the stresses and displacements of a multi-layered road structure.

3.3. *Formulation of cumulative deformation*

From the model experiment conducted in Section 2, it is found that the total cumulative deformation of road structure layers themselves is not great after one million repeated loadings. However, for a road constructed on soft subsoil, the cumulative deformation generated by the soft subsoil could be great, especially for the road with low embankment constructed on soft soil since the dynamic deviator stress of soft soil caused by traffic loads is larger for low road embankment than other ones, and the compressible soft soil layer could also be thicker. Therefore, it is significant to study the traffic-load-induced cumulative deformation of both road infrastructures and their soft subsoil. In this section, the cumulative plastic deformation of the road on the soft subsoil S_{p} is calculated according to the following formula:

$$S_{\mathrm{p}} = S_{\mathrm{p1}} + S_{\mathrm{p2}} = \sum_{i=1}^{m} \kappa_i N^{\chi_i} h_i + \sum_{j=1}^{n} \varepsilon_{pi} H_i, \tag{35}$$

in which S_{p1} is the deformation of road structure layers themselves; it can be calculated according to the results of the model experiment of Section 2, κ_i and χ_i are experimental parameters shown in Table 5, h_i and m are the thickness and number of the structure layers, respectively. $S_{p2} = \sum_{i=1}^{n} \varepsilon_{pi} H_i$ is the deformation of the soft subsoil, here, ε_{pi} is the cumulative plastic strain of each compressible layer of subsoil, and H_i is the thickness of each compressible layer of subsoil. An empirical equation for calculating the cumulative plastic strain of cohesive soils under repeated loading, proposed by Li and Selig (1996), has been used to determine the cumulative plastic strain of each compressible layer ε_{pi} in present study.

$$\varepsilon_p = a \left(\frac{q_d}{q_f} \right)^k N^b, \tag{36}$$

where q_d is the vehicle-induced dynamic deviator stress of subsoil determined by the stress components $(\sigma_{rr}, \sigma_{\theta\theta}, \sigma_{zz}, \sigma_{rz})$ which can be derived by the dynamic stiffness matrix method developed in Section 3.1.

$$q_d = \sqrt{\tfrac{1}{2}[(\sigma_{zz} - \sigma_{rr})^2 + (\sigma_{zz} - \sigma_{\theta\theta})^2 + (\sigma_{rr} - \sigma_{\theta\theta})^2 + 6\sigma_{rz}^2]}, \tag{37}$$

where N is the number of repeated loading applications, a, k and b are experimental constants which are related to the plasticity index of subsoil and the suggested values are as in Table 6 proposed by Li and Selig (1996), q_f is the static failure deviator stress and can be measured by a

Table 6. Experimental constants of different subsoil types.

Soil type	*a*	*b*	*k*
Low-plasticity silt	0.64	0.10	1.7
High-plasticity silt	0.84	0.13	2.0
Low-plasticity clay	1.10	0.16	2.0
High-plasticity clay	1.20	0.18	2.4

field vane shear test or determined by the following the empirical equation (Chai & Miura, 2002).

$$q_f = \frac{2c_{cu}\cos\varphi_{cu}}{(1-\sin\varphi_{cu})} + \frac{(1+K_0)\sigma_{cz}\sin\varphi_{cu}}{(1-\sin\varphi_{cu})}, \tag{38}$$

where c_{cu} and φ_{cu} are the cohesion force and internal friction angle of the soft subsoil, respectively, K_0 is the horizontal earth pressure coefficient and σ_{cz} is the gravity stress of the soft subsoil.

From Equations (35)–(38), one can calculate the traffic-load-induced cumulative deformation of both road structures and the soft subsoil.

3.4. *Numerical results and discussion*

In this section, a computing model of a multi-layered road structure on soft subsoil is built to study the cumulative deformation of a road structure subjected to vehicle traffic loads, as shown in Figure 10. In accordance with the experimental section, the computing model is divided into a multi-layered system composed of surface layer, base layer, sub-base layer, subgrade layer and soft subsoil half-space. Because the properties of the three sub-layers of subgrade have little difference (as shown in Table 2), the subgrade in Figure 10 is simplified as a single layer whose elastic modulus is 35 MPa and thickness is 1.05 m. Other physical and mechanical characteristics of road structure layers are the same as presented in Table 2. In terms of soft subsoil, Shanghai clay deposit is adopted for calculating the cumulative plastic deformation, and the subsoil parameters

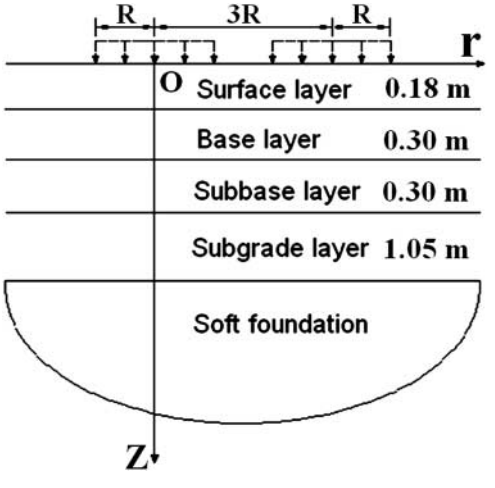

Figure 10. Model for a multi-layered road structure on soft subsoil.

Table 7. Subsoil parameters of Shanghai clay deposit.

Subsoil layer	Depth (m)	Unit weight (kN/m^3)	Cohesion force (kPa)	Internal friction angle (°)	Horizontal earth pressure coefficient
Clay layer 1	0–0.8	18.2	13.6	13.0	0.76
Clay layer 2	0.8–7.3	17.8	19.0	7.0	0.67
Silt clay 1	7.3–19.7	16.9	7.8	10.0	0.86
Silt clay 2	19.7–22.4	18.3	20.0	6.0	0.66

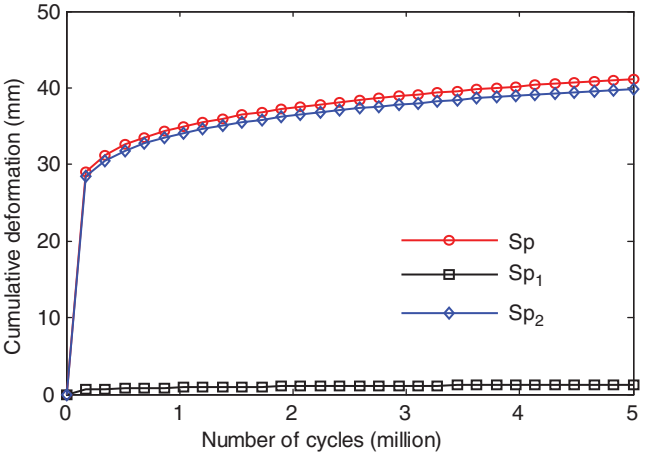

Figure 11. Development of cumulative deformation with the number of cycles.

are listed in Table 7 (Li, Huang, & Wang, 2006). The soft subsoil is considered as elastic half-space medium and its elastic modulus and density are 10 MPa and 1750 kg/m^3, respectively. Some numerical results are derived through solving Equations (35)–(38).

In order to explain the different deformations of road structure layers themselves (S_{p1}) and the soft subsoil (S_{p2}), the cumulative deformations S_{p1}, S_{p2} and S_p are plotted respectively versus the number of repeated loading applications until five million cycles, and are shown in Figure 11. It is seen that the traffic-load-induced cumulative deformation of road structure layers themselves S_{p1} is much smaller than that of soft subsoil S_{p2}, and the total cumulative deformation S_p is mainly generated by the soft soils. It can also be seen from Figure 11 that the cumulative deformation of road structure increases very fast for a short number of cycles and becomes much lower with the increasing of repeated loading number.

Providing that the loads move along the centreline of the road, Figure 12 presents the distribution of cumulative deformation of crossroad profile after one million cycles, where different depths including 0.0, 1.0, 1.5 and 2.5 m below the subgrade surface are considered. As can be seen, the values of cumulative deformation of different depths decrease sharply along the horizontal direction, then gradually decrease to zero when far away from the road centreline by more than 5 m. It should be noted that the maximum cumulative deformation of 2.5 m below the subgrade surface is significantly smaller than that of the subgrade surface, which indicates that the traffic-load-induced cumulative deformation is mainly generated by the superficial layer of soft subsoil.

The effects of the stiffness and thickness of the road base and subgrade on the total cumulative deformation are investigated as shown in Figures 13–15. It is obvious that the variations of cumulative deformation in different situations (base modulus with 700, 1000 and 1400 MPa;

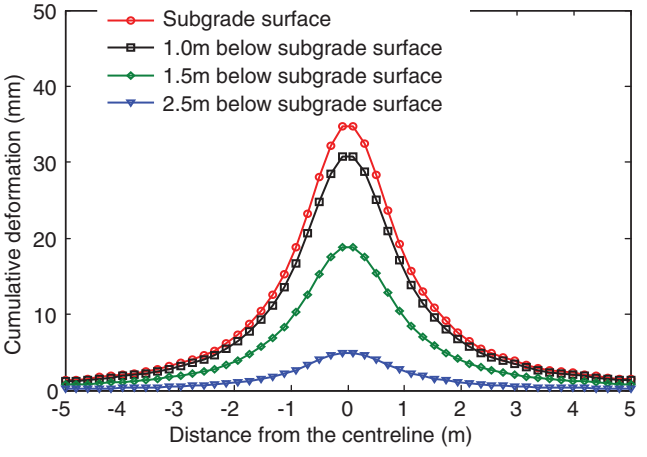

Figure 12. Variation of cumulative deformation with depth at one million cycles.

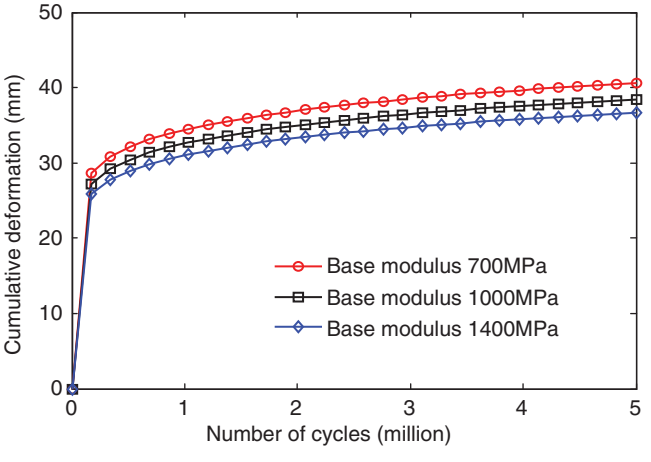

Figure 13. Effect of base modulus on cumulative deformation.

subgrade modulus with 30, 50 and 70 MPa and subgrade thickness with 1.0, 1.5, 2.0 and 2.5 m) are similar as Figure 11. The cumulative deformation of the road decreases with the increasing of stiffness and thickness of the road base and subgrade. Compared with Figures 13 and 15, the effect of subgrade thickness on the road cumulative deformation which is shown in Figure 14 is more considerable.

In Figure 16, the influence of two different subsoil types on the cumulative deformation are compared, which correspond to different values for a, m and b as shown in Table 6. It can be seen that the traffic-load-induced cumulative deformation of road constructed on low plasticity silt ground is much smaller than that of high plasticity clay ground after several million cycles since it is more difficult to be compressed for high-plasticity clay layer. Thus, on soil with high plasticity such as clay, it is effective to reinforce and stabilise the subsoil for the sake of reducing the cumulative plastic deformation.

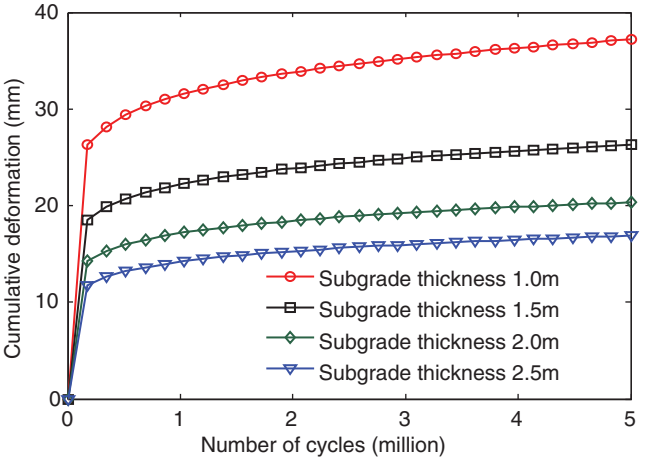

Figure 14. Effect of subgrade thickness on cumulative deformation.

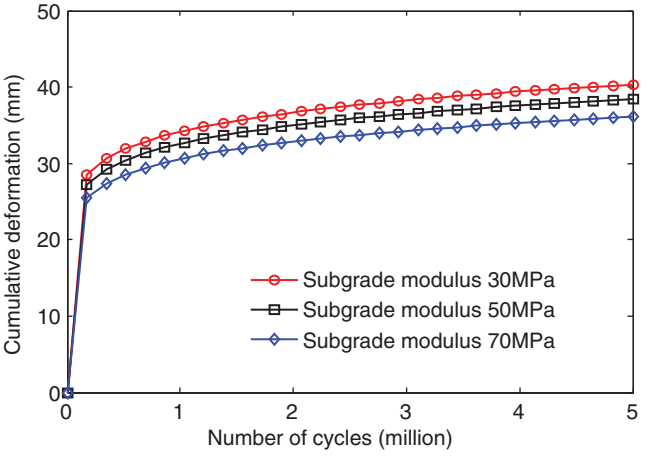

Figure 15. Effect of subgrade modulus on cumulative deformation.

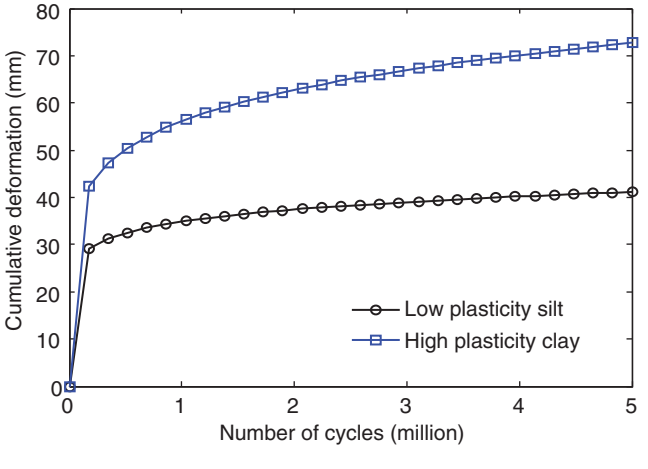

Figure 16. Effect of subsoil types on cumulative deformation.

4. Conclusion

In this paper, the traffic-load-induced stress, displacement and cumulative plastic deformation of a multi-layered road structure is investigated based on the laboratory model experiment and theoretical analysis. A physical model with thin asphalt surfacing layer, cement-stabilised gravel road base and layered decomposed granite soil subgrade is built to better understand the dynamic behaviour of the road structure system. Experiments are performed to determine the elastic responses and used to verify the theoretical solutions obtained from an exact stiffness matrix approach and an assembly process. Then a new method is proposed to predict traffic-load-induced cumulative deformation of both road structure layers and soft subsoil. Some numerical results are also presented for illustrations.

Comparisons of the calculated results with the laboratory model experiment ones indicate that the traffic-load-induced stress components, which are very important in predicting the cumulative deformation of road structure, can be calculated by using a stiffness matrix approach to deal with the multi-layered system. The experimental and numerical results of the elastic responses showed a relatively good agreement, although at small distances, the numerical response was underestimated. This validates that the stiffness matrix method is useful in predicting the stresses and elastic deformations of a multi-layered road structure.

Then, a method for predicting traffic-load-induced cumulative deformation of a road structure on soft subsoil is proposed on the basis of the elastodynamic theory for a multi-layered system and an empirical equation for soft cohesive soils. The proposed method is reasonable in predicting the traffic-load-induced cumulative deformation and can be used to calibrate the design of the road on soft subsoil with a low embankment. The analysis also revealed the following three points: (1) the majority of the stresses caused by vehicle traffic loads are imposed and dispersed by the road pavement; (2) for the road constructed on soft soil, the traffic-load-induced cumulative deformation of road structure layers is mainly generated from the soft subsoil and (3) subgrade thickness and subsoil type are two of the most important factors controlling the traffic-load-induced cumulative deformation of a road constructed on soft soils.

Acknowledgements

The work presented in this paper is supported by the National Natural Science Funds (Grant No. 51209201 and 51279198) and the Twilight Science Project Foundation of Wuhan (No. 201150431070). Constructive comments from the anonymous referees are highly appreciated.

References

Akbulut, H., & Aslantas, K. (2005). Finite element analysis of stress distribution on bituminous pavement and failure mechanism. *Materials and Design*, *26*, 383–387.

Chai, J., & Miura, N. (2002). Traffic-load-induced permanent deformation of road on soft subsoil. *Journal of Geotechnical and Geoenvironmental Engineering*, *128*, 907–916.

China Communications Press. (1996). *Technical specifications for design and construction of highway embankment on soft ground* (JTJ017-96). Beijing: Author.

China Communications Press. (2006). *Specifications for design highway asphalt pavement* (JTGD50-2006). Beijing: Author.

China Communications Press. (2007). *Test method of soils for highway engineering* (JTG E40-2007). Beijing: Author.

Ferrari, J., Perciante, D., & Dubra, A. (1999). Fast Hankel's transform of nth order. *Journal of the Optical Society of America A*, *16*, 2581–2582.

Francois, S., Karg, C., Degrande, G., & Haegeman, W. (2010). A numerical model for foundation settlements due to deformation accumulation in granular soils under repeated small amplitude dynamic loading. *International Journal for Numerical and Analytical Methods in Geomechanics*, *34*(3), 273–296.

Fujikawa, K. (1996). *On optimistic design of low embankment road on soft subsoil by considering the traffic-load-induced settlement*. Saga: University of Saga.
Fujikawa, K., Miura, N., & Beppu, I. (1996). Field investigation on the settlement of low embankment road due to traffic load and its prediction. *Soils and Foundations*, *36*, 147–153.
Hu, Y. Y. (2010). Long-term settlement of soft subsoil clay under rectangular or semi-sinusoidal repeated loading of low amplitude. *Canadian Geotechnical Journal*, *47*(11), 1259–1270.
Hyodo, M., Yasuhara, K., & Murata, H. (1996, April). *Deformation analysis of the soft clay foundation of low embankment road under traffic loading*. Proceedings of 31st symposium of Japanese Society of Soil Mechanics and Foundation Engineering, Tokyo.
Joseph, A., & James, M. (2012). Permanent deformation testing for a new South African mechanistic pavement design method. *Construction and Building Materials*, *26*, 541–546.
Kettil, P., Lenhof, K., & Runesson, N. (2007). Simulation of inelastic deformation in road structures due to cyclic mechanical and thermal loads. *Computers and Structures*, *85*, 59–70.
Kutara, K., Miki, H., & Mashita, Y. (1980). Settlement and countermeasures of the road with low embankment on soft ground. *Technical Report Civil Engineering*, *22*, 13–16.
Lefeuve-Mesgouez, G., & Mesgouez, A. (2012). Three-dimensional dynamic response of a porous multilayered ground under moving loads of various distributions. *Advances in Engineering Software*, *46*, 75–84.
Li, D., & Selig, E. (1996). Cumulative plastic deformation for fine-grained subgrade soils. *Journal of Geotechnical Engineering*, *122*, 1006–1013.
Li, D., & Selig, E. (1998). Method for railroad track foundation design, II: Application. *Journal of Geotechnical Engineering*, *124*, 323–329.
Li, J., Huang, M., & Wang, Y. (2006). Analysis of cumulative plastic deformation of soft clay foundation under traffic loading. *China Journal of Highway Transportation*, *19*, 1–5.
Lu, Y., & Wright, P. (1998). Numerical approach of visco-elastoplastic analysis for asphalt mixtures. *Computers and Structures*, *69*, 139–147.
Manzari, M., & Prachathananukit, R. (2001). On integration of a cyclic soil plasticity model. *International Journal for Numerical and Analytical Method in Geomechanics*, *25*, 525–549.
Monismith, C., Ogawa, N., & Freeme, C. (1975). Permanent deformation characteristics of subgrade soils due to repeated loading. *Transportation Research Record*, *537*, 1–17.
Mulungye, R., Owende, P., & Mellon, K. (2007). Finite element modelling of flexible pavements on soft soil subgrades. *Materials and Design*, *28*, 739–756.
Su, X., Tian, J., & Pao, Y. (2002). Application of the reverberation-ray matrix to the propagation of elastic waves in a layered solid. *International Journal of Solids and Structures*, *39*, 5447–5463.
Wang, W., & Ishikawa, H. (2002). A method for linear elasto-static analysis of multi-layered axisymmetrical bodies using Hankel's transform. *Computational Mechanics*, *27*, 474–483.
Yao, H. L., Lu, Z., & Luo, H. N. (2009). Dynamic response of rough pavement on Kelvin foundation subjected to traffic loads. *Rock and Soil Mechanics*, *30*(4), 890–896.
Zeng, L., Olsson, J., & Wiberg, N. (2000, September). *Road mechanics-finite element analysis of a multi-physics problem*. Proceedings of European congress on computational methods in applied sciences and engineering, Barcelona.